SCIENTIFIC REPORTS

OPEN

SUBJECT AREAS:
PLANT DEVELOPMENT
PLANT ECOLOGY

Received
20 March 2014

Accepted
14 May 2014

Published
3 June 2014

Correspondence and requests for materials should be addressed to E.V.G. (egorb@zoologie.uni-kiel.de)

Adhesion force measurements on the two wax layers of the waxy zone in *Nepenthes alata* pitchers

Elena V. Gorb, Julia Purtov & Stanislav N. Gorb

Department of Functional Morphology and Biomechanics, Zoological Institute, Kiel University, Am Botanischen Garten 9, 24098 Kiel, Germany.

The wax coverage of the waxy zone in *Nepenthes alata* pitchers consists of two clearly distinguishable layers, designated the upper and lower wax layers. Since these layers were reported to reduce insect attachment, they were considered to have anti-adhesive properties. However, no reliable adhesion tests have been performed with these wax layers. In this study, pull-off force measurements were carried out on both wax layers of the *N. alata* pitcher and on two reference polymer surfaces using deformable polydimethylsiloxane half-spheres as probes. To explain the results obtained, roughness measurements were performed on test surfaces. Micro-morphology of both surface samples and probes tested was examined before and after experiments. Pull-off forces measured on the upper wax layer were the lowest among surfaces tested. Here, contamination of probes by wax crystals detached from the pitcher surface was found. This suggests that low insect attachment on the upper wax layer is caused primarily by the breaking off of wax crystals from the upper wax layer, which acts as a separation layer between the insect pad and the pitcher surface. High adhesion forces obtained on the lower wax layer are explained by the high deformability of probes and the particular roughness of the substrate.

Carnivorous plants have adapted to grow in nutrient poor habitats and derive lacking nutrients from trapping and consuming animals[1]. Plants from the genus *Nepenthes* rely on the capturing success of their passive trapping organs called pitchers. Insects with both smooth attachment pads consisting of compliant material and hairy attachment pads bearing fibrillar surface structures[2–4] can be trapped by pitchers, however, ants (smooth pads) comprise the main prey of most *Nepenthes* species[5–7].

Pitchers of *Nepenthes* plants are composed of several zones, such as the leaf-like lid, ribbed peristome, waxy zone, transitional zone lacking specialized surface structures and digestive zone with numerous digestive glands[8,9]. These zones show different macro-morphologies as well as surface micro-architectures and play different roles in attracting, trapping, retaining and digesting of animal prey (see the review by Moran and Clarke[10]).

Nepenthes pitchers employ different trapping and retention mechanisms. The contribution of the waxy zone for trapping and retaining functions has been repeatedly reported[1,9,11–20]. During the past decade, the role of water-lubricated peristome surface[21,22] and highly viscous trapping fluid[23,24] for prey capturing was discovered. For a number of species, the relative contributions of the most widespread trapping structures, such as the peristome, wax crystals and viscous fluids, were recently inverstigated[20,25,26].

In many *Nepenthes* species, the waxy zone situated inside the pitcher, just below the peristome (Fig. 1A), bears lunate cells (downward directed modified stomata), decreasing in number towards the pitcher's base, and a thick epicuticular wax coverage, which may consist of several layers of wax crystals[1,9,11–20,27]. Our studies on *N. alata* revealed two easily distinguishable, superimposed wax layers, the upper and lower layers, differing in micro-structure, chemical composition and mechanical properties[13,15,20,27]. The lower layer has a foam-like structure and is composed of interconnected membranous platelets. Irregular cavities occur between these crystals, positioned at acute angles relative to the pitcher wall surface. The upper layer consists of densely placed, separate irregular platelets arranged perpendicularly to the subjacent layer. Platelets of the upper and lower wax layer are connected to one another by thin stalks.

Attachment ability of insects with both smooth and hairy adhesive pads was examined using locomotion experiments, in which insects either were unable to move or walked very slowly and covered extremely small distances on the upper wax layer of the intact waxy zone[9,28]. No such experiments were performed on the lower wax layer. In addition, traction forces were measured for insects with both types of adhesive pads on the upper

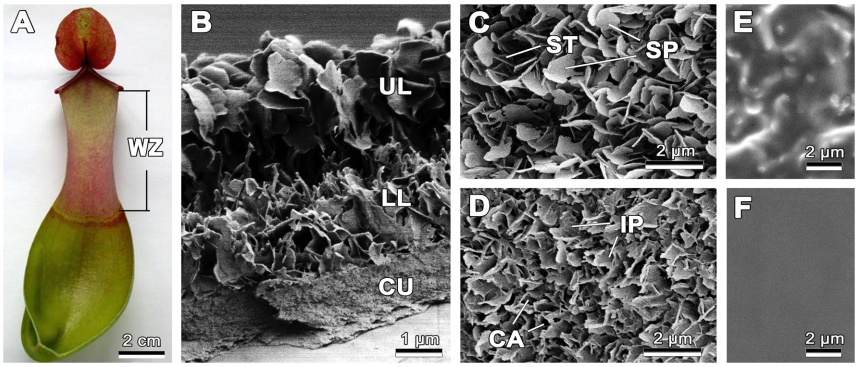

Figure 1 | Micro-morphology of test surfaces. (A) Longitudinally dissected pitcher of *N. alata*. (B) Fracture of the wax coverage in the waxy zone, consisting of two layers, the upper and the lower wax layer. (C) Top view of upper wax layer where separate platelet-shaped wax crystals bearing thin stalks are clearly visible. (D) Top view of the lower wax layer, composed of interconnected platelets with cavities in-between. (E) Micro-rough epoxy resin replica with an asperity size of 3 µm. (F) Smooth epoxy resin replica. CA, cavities; CU, cuticle; IP, interconnected membranous platelets; LL, lower layer; ST, stalks; SP, separate irregular platelets; UL, upper wax layer; WZ, waxy zone. (B–D) Cryo-SEM micrographs. (E,F) SEM micrographs.

wax layer[13,17,19], but only for insects with hairy pads on the lower layer[13]. In all of these experiments, traction forces were strongly reduced on the waxy layers as compared with those on wax free surfaces.

According to our previously proposed hypotheses[29], a reduction of insect adhesion on a plant surface covered with a 3D crystalline epicuticular wax may be explained by (1) the decrease of real contact area between the insect adhesive pads and the plant substrate caused by surface micro-roughness (roughness-hypothesis); (2) the absorption of the pad fluid by the structured wax coverage (fluid-absorption-hypothesis); (3) the dissolving of the wax crystals by the pad secretion, resulting in substrate slipperiness and hydroplaning (wax-dissolving-hypothesis); (4) the contamination of pads by wax crystals (contamination-hypothesis). For the *N. alata* waxy pitcher surface, the decrease in insect attachment ability was explained by prevention of insect adhesion via reduction of the real contact area[9,13,17,18] and/or contamination[1,11,13,28,30]. Also, due to the fragile and brittle nature of wax crystals and their small dimensions, insects are not able to apply their claws for interlocking with crystals in order to climb up the pitcher wall[17].

Although a number of studies have reported on the anti-attachment effect of the *N. alata* wax coverage on insects and discussed different mechanisms contributing to the anti-adhesive function[1,9,11,13,17,18,28,30], adhesion force measurements on these surfaces have not been performed. This was mainly due to the absence of a reliable and sensitive method for testing surfaces with very low adhesive capabilities. Using a newly developed experimental approach[31] and applying polydimethylsiloxane (PDMS) half-spherical indenters with elastic properties similar to those of the smooth adhesive pads in insects, we carried out pull-off force measurements on the lower and upper wax layers in the waxy zone of *N. alata* pitchers. The aim of our study was to estimate the adhesion properties of these layers. This information is essential to understand details of the trapping mechanism of the upper wax layer.

Results

Micro-morphology of test surfaces. The fractured wax coverage in the intact waxy zone confirmed our previous findings[13,15,20,27] about the composite structure of two superimposed wax layers on the top of the cuticle in *N. alata* pitchers (Fig. 1B). The top views of the wax layers' surfaces displayed further details of the wax structure. The lower wax layer resembled foam and was composed of membranous platelets with irregularly-shaped cavities in-between (Fig. 1D). The upper layer emerged as separate irregular platelet-shaped wax crystals without a regular pattern (Fig. 1C). Thin stalks connected the platelets of the upper layer with the lower wax layer. Surfaces of the smooth and micro-rough epoxy resin replicas are shown in Fig. 1E,F.

Surface roughness. The standard roughness parameters (mean roughness R_a, root mean square of roughness r.m.s., and the maximum height of the profile R_z) of the tested samples, apart from the smooth replica, were relatively similar in their values (Table 1). Further analysis of topographical data in the rough surfaces showed two types of roughness, influenced by either (1) one wavelength (micro-rough replica) (Fig. 2A,B) or (2) two wavelengths (both plant surfaces) (Fig. 2C–F). While the one-wavelength type was represented by coarse domains with a smooth surface on hills and in valleys, the two-wavelength type was composed of one wavelength with a high frequency and low amplitudes caused by the wax coverage and a second wavelength with a low frequency and high amplitudes due to the epidermal cells' topography (Fig. 2D,F). High-frequency filtering of roughness data (not shown) supported these two types of roughness characters.

Pull-off forces. Absolute pull-off force values obtained on different test surfaces in the first type of experiment (three single measurements with each probe on the smooth replica, micro-rough replica, and one of the wax layer samples) are presented in Table 1. We obtained significantly different normalized pull-off forces on tested samples (normality test: failed, $P < 0.050$; Friedman repeated measures ANOVA on ranks: $X^2 = 39.6$, d.f. = 3, P = 1.3482E-8; Table 2 and Fig. 3A). Among all surfaces, the upper wax layer showed the lowest force. Forces on both the upper wax layer and micro-rough replica were significantly lower than those on the smooth replica and lower wax layer. As for the latter two samples, pull-off force on the lower layer was slightly higher compared to the smooth surface.

In the second type of experiment (three single measurements with the same probe on the smooth sample, upper wax layer, and again the smooth sample), the comparison of normalized forces obtained in the first and second tests on the smooth sample showed no significant difference (normality test: passed, P = 0.069; paired t-test: t = 0.570, d.f. = 14, P = 0.578; Fig. 3B).

The effective E-modulus of polymer probes amounted to a value of 49.47 ± 13.99 kPa at a mean applied force of 697.27 ± 129.59 µN (n = 40). Using this value in equations, we obtained pressure values of $p_{min} = 138.07$ Pa for 0.5 mN applied force and $p_{max} = 173.96$ Pa for 1 mN applied force.

Effects of adhesion experiments on surfaces of samples and probes. Scanning electron microscopy (SEM) investigations of

Table 1 | Geometrical characteristics of test surfaces and absolute pull-off force values obtained on different test surfaces. n, number of measurements; R_a, mean roughness; r.m.s., root mean square of roughness; F_{off}, pull-off force; R_z, maximum height of the profile. Data are presented as mean ± s.d

Surface	R_a [μm]	r.m.s. [μm]	R_z [μm]	F_{off} [mN]
Smooth replica	0.007 ± 0.001 n=6	0.009 ± 0.001 n=6	0.069 ± 0.035 n=6	3.372 ± 0.587 n=40
Micro-rough replica	1.329 ± 0.138 n=6	1.685 ± 0.172 n=6	11.550 ± 0.630 n=63	2.609 ± 0.891 n=40
Upper wax layer	1.909 ± 0.247 n=6	2.378 ± 0.301 n=6	27.112 ± 1.728 n=6	0.847 ± 0.493 n=18
Lower wax layer	1.831 ± 0.715 n=6	2.229 ± 0.810 n=6	13.013 ± 4.120 n=6	4.364 ± 1.563 n=22

samples and probes performed after pull-off force measurements demonstrated that, with the exception of the upper wax layer, changes neither of the test surface nor of the probe topography occurred during experiments (Fig. 4B). In the case of the upper wax layer, a strong contamination of probes used in measurements was shown (Fig. 4A). Contaminated areas were covered with wax particles arranged in clusters corresponding to the pattern of epidermal cells (Fig. 4D). Further magnification showed a conspicuous shape of adhering wax crystals (Fig. 4F) similar to that observed in the intact upper layer (Fig. 1C). The wax structures on the contaminated probes were composed of platelets with regular margins and rather long, thin shafts, reaching from half to full size of the crystal platelets. The surface of these platelets was not completely smooth, but had a particular roughness due to an apparent folding. Apart from distinct wax crystals, smaller wax particles were found in the contact area. This indicates the fragile nature of crystals in the upper wax layer. We also observed some changes in the plant surface after the experiments (Fig. 4C,E). The contact zone lacked the upper wax layer and displayed a wax structure with irregular membranous platelets and cavities resembling the lower wax layer (Fig. 4G).

Discussion

Using a newly developed measuring method[31], we characterized adhesive properties of the two wax layers in the waxy zone of the *N. alata* pitcher. It is well known that adhesive properties of biological surfaces are greatly affected by a number of factors, above all by surface topography[17,18,29,32,33]. Therefore, in addition to pull-off force measurements, we performed a detailed characterization of surface samples, including structural analysis and roughness measurements. Also, mechanical properties of counterparts strongly influence adhesion. Here, by using tacky half-spherical PDMS probes[31] having an elasticity modulus of $E = 50$ kPa, we simulated the material of smooth adhesive pads in insects. For this type of attachment device, elasticity moduli of 27 kPa in *Tettigonia viridissima* (Orthoptera, Tettigoniidae)[34] and 12–625 kPa in *Carausius morosus* (Phasmatodea)[35] have been previously reported. Moreover, we applied a normal force ranging from 500 to 1000 μN resulting in a pressure of $p_{min} = 138.07$ Pa and $p_{max} = 173.96$ Pa, respectively. According to data in the literature[17], in a typical prey such as an ant, the contact area of a single adhesive organ (arolium) is about 10000 μm^2. For a middle-sized ant, weighing 3 mg and having from three to six feet in contact, we obtain a pressure of $p_{6feet} = 83$ Pa to $p_{3feet} = 327$ Pa. Thus, the pressure applied in the present study was within the range of that of a typical *Nepenthes* pitcher's prey.

We are aware that soft PDMS half-spheres lack several of the complex features of insect attachment devices, such as the presence of a secretion, a complex ultra-structure, a gradient in material properties and a pair of claws. However, the strength of our approach lies in the testing of the interaction between an adhesive material and *Nepenthes* wax layers under exactly defined conditions, such as the precise contact geometry and material properties of the adhesive counterpart as well as biologically relevant contact pressure. The following discussion is devoted to the interpretation of our experimental results from the biological perspective.

Lower wax layer. The observations of other authors and our own previous experimental data showed the ability of platelets from the

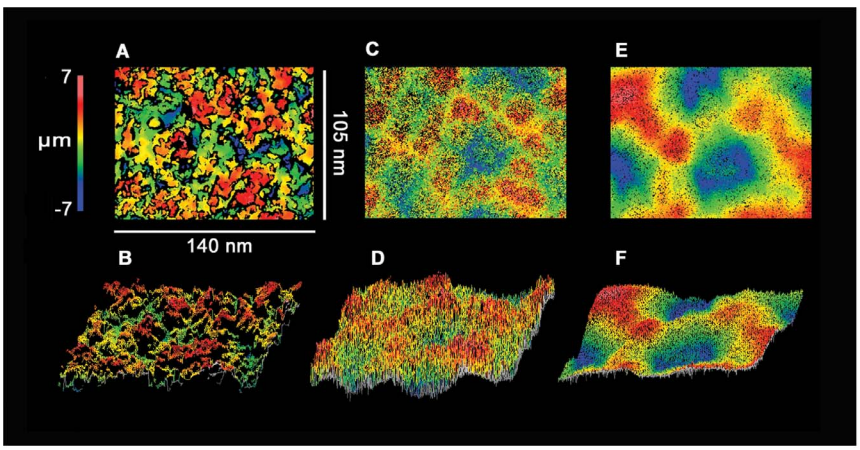

Figure 2 | Images of rough test surfaces obtained with white light interferometer. (A,B) One-wavelength roughness of the micro-rough replica represented by coarse domains with a smooth surface on hills and in valleys. (C–F) Two-wavelength roughness of the upper wax layer (C,D) and the lower wax layer (E,F) showing combined roughness patterns due to the presence of wax crystals and epidermal cells. (A,C,E) Height maps. (B,D,F) 3D oblique maps.

Table 2 | Results of multiple pairwise comparisons (Wilcoxon signed rank test with Bonferroni correction) of normalized pull-off forces obtained on different surfaces. LL, lower wax layer; rough, micro-rough epoxy resin replica; P, Bonferroni corrected probability value; smooth, smooth epoxy resin replica; UL, lower layer

Comparison	P	Difference
Smooth vs rough	6.638E-4	yes
Smooth vs LL	1.000	no
Smooth vs UL	6.866E-5	yes
Rough vs LL	9.499E-3	yes
Rough vs UL	6.866E-5	yes
LL vs UL	6.866E-5	yes

upper wax layer to contaminate the feet of insects during their contact with the waxy zone[11,13,28]. Removal of the upper wax layer platelets from the pitcher surface should partially expose the lower layer, which can then contribute to the trapping mechanism. Moreover, since the upper wax layer is unable to regenerate[27], the lower wax layer might be a kind of supplementary system supporting the trapping function of thus damaged areas of the waxy zone. Another reason for investigating the adhesive properties of the lower wax layer was to evaluate the biological significance of the upper wax layer (i.e. if the upper wax layer is missing, would the pitcher still be able to trap insects).

Pull-off forces measured on the lower wax layer were non-significantly higher than those on the smooth surface. This result might be explained by the general presumption that adhesion forces are proportional to the area of real contact between surfaces[36], as has already been supported by various authors[37–39]. Similar force values obtained on the lower wax layer and smooth surface suggest a similar real contact area between probes and the two surfaces. On the lower wax layer in contact with the probe, a real contact area comparable to that on the smooth surface is probably achieved by a partial inflow of the probe material, having a low E-modulus, into the cavities between wax crystals (Fig. 5D). A slight trend for higher forces on the lower wax layer might be also due to pinning of probes by stiff, pointed and irregular crystal margins and/or some additional friction and interlocking effects. Also, a possible chemical effect of the fluid polyvinylsiloxane used to expose the lower wax layer cannot be entirely excluded.

High adhesion forces achieved on the lower layer are not in line with previous data[13], which described an anti-attachment effect not only for the upper, but also for the lower wax layer. These experiments, however, were performed with tethered ladybird beetles bearing hairy attachment pads. A recent atomic force microscopy study of ladybird beetle setae showed the lowest E-modulus of 1 MPa at the setal tip[40]. Thus, the material in these hairy adhesive pads is much stiffer than that in smooth pads. For this reason, the inflow

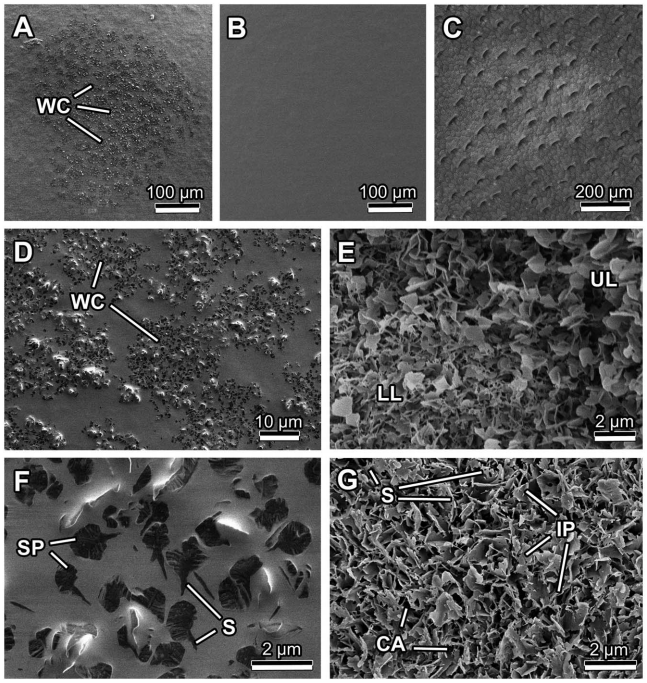

Figure 4 | Cryo-SEM micrographs of polymer probes (A,B,D,F) and plant samples (C,E,G) after adhesion experiments. (A) Surface of the probe highly contaminated with wax crystals after being in contact with the upper wax layer. (B) Clean (non-contaminated) probe surface after contact with the lower wax layer. (C) The area of the waxy zone after being in contact with the sticky probe in an adhesion experiment. The contact zone has a whitish appearance due to changes in the wax coverage. (D) On the contaminated surface of the probe, wax crystals are arranged in clusters corresponding to the pattern of epidermal cells. (E) The border between the intact upper layer and the contact zone showing the remaining lower layer of wax. (F) The probe surface shown in (D) at high magnification. Adhered wax crystals are similar to those from the upper wax layer: platelets having a fine ridged structure and bearing thin stalks. (G) The contact zone with the lower wax layer after detachment from the probe. CA, cavities; IP, interconnected membranous platelets; LL, lower layer; S, stalks; SP, separate irregular platelets; UL, upper layer; WC, wax crystals.

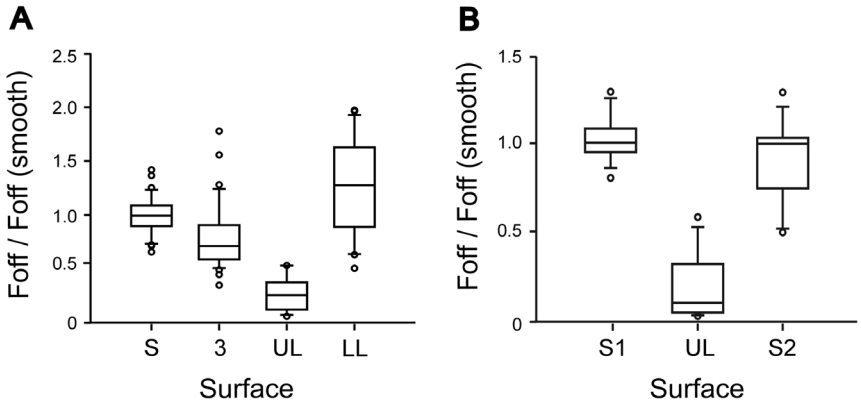

Figure 3 | Normalized pull-off forces obtained on different surfaces in the first (A) and second (B) type of experiment. The ends of the boxes define the 25th and 75th percentiles, with a line at the median and error bars defining the 10th and 90th percentiles. Circles indicate outliers. 3, rough epoxy resin replica having 3 µm asperity size; LL, lower wax layer; S, smooth replica; S1, smooth sample before contact with the wax surface; S2, smooth sample after contact with the wax surface; UL, upper wax layer.

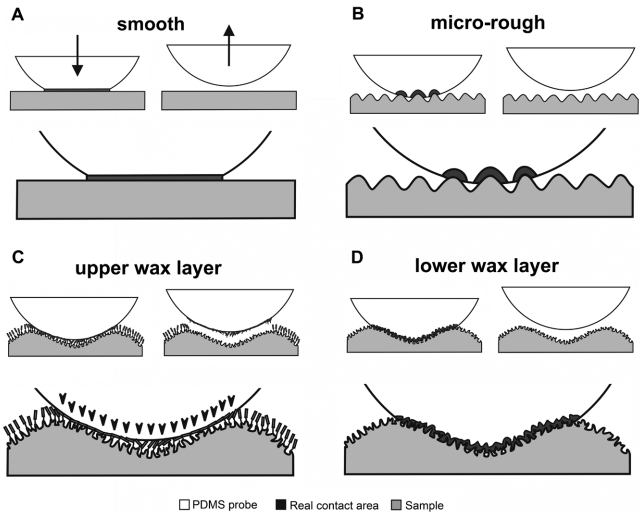

Figure 5 | Scheme explaining hypothetical surface interactions between different samples and soft adhesive probes. (A) On a smooth replica, full contact occurs. (B) On a micro-rough sample, the real contact area is reduced due to the formation of partial contacts. (C) A complex interaction of a probe with the intact waxy zone containing both upper and lower wax layers: the surface of the probe is contaminated with upper wax layer crystals, serving as a separation layer. (D) The probe follows the surface's profile of the lower wax layer resulting in a real contact area comparable to that on the smooth surface.

effect of pad material into the cavities between wax crystals may not occur for hairy systems, but might happen in the case of smooth systems. Unfortunately, no attachment experiments on the lower wax layer have been done with insects equipped with smooth attachment devices. We hypothesize that some insects with smooth adhesive pads would be able to walk on the lower wax layer of *N. alata*. To test this hypothesis, further experiments have to be performed.

Apparently, the standard roughness parameters (R_a, r.m.s., R_z) were not sufficient to describe peculiarities of the surface topography in detail. While the measured roughness parameters of the lower wax layer and micro-rough replica were very similar, pull-off forces differed significantly. This effect might be explained by the different character of recorded roughness, displayed in white light interferometer (WLI) oblique 3D plots (see Fig. 2B,F). The soft probe material might adapt well to both wavelengths of the lower wax layer topography, such as the short wavelength with low amplitudes caused by wax crystals and the longer wavelength with high amplitudes caused by epidermis cells (Fig. 5D). The wavelength of the micro-rough replica has a middle range amplitude compared to that of the lower wax layer. At this range, the probe might be not able to follow the topography of the surface. As a result, a number of partial contacts would occur and this would lead to a lower real contact area (Fig. 5B). The significantly lower pull-off force obtained on the micro-rough surface compared to the lower layer sample might indicate that insects bearing smooth attachment pads are less effective on this particular domain dimension of the surface structure.

Upper wax layer. The strong reduction of pull-off force on the upper wax layer compared to all other tested surfaces might be explained primarily by the breaking off of wax crystals from the upper wax layer that acts as a separation layer and also contaminate the sticky half-spheres (Fig. 5C). The contaminating effect of *N. alata* wax crystals has also been previously reported by other authors[1,11,13,28], but was recently rejected by Scholz et al.[17]. We discovered here that the contaminating material on the probes and the remaining wax structures found at the contact area on the plant surface after adhesion experiments clearly showed certain similarities to the wax crystals from the upper and lower layers, respectively. Furthermore, these detached platelets had rather long stalks. This supports the previous conclusion that the connection between the superimposed upper wax layer and the underlying surface structure might be due to thin breakable stalks[13,30]. Analysis of the fracture behavior of epicuticular wax crystals, performed using a mathematical approach, was recently undertaken by Borodich et al.[41]. The authors showed the possibility of wax crystals breaking under the weight of an insect. We have observed a rather small amount of fractured crystal parts on the contaminated probes. This might be an indication that the stalks act as predeterminated breaking points.

We suggest that the breaking off of wax crystals from the upper wax layer is important primarily for decreasing attachment forces during the very first contact with the wax coverage (Fig. 5C). In this case, detached crystals serve as a separation layer between counterparts (the pitcher surface and insect pad), thus causing the adhesion reduction and slipperiness of the surface. Such an effect of a separation layer is well known in surface physics[42,43].

We also hypothesized that the contamination might also impede insect pad adhesion during further contacts. This means that after detached platelets from the upper layer covered a rather large area on the pad and formed a micro-rough surface there, contact would occur between the micro-rough pad surface and stiff micro-rough lower wax layer of the plant. As the adhesion force directly depends on the real contact area, it would be low in this case. However, our results obtained in the second type of experiment showed that the amount of contamination after the first contact of the PDMS probe with the upper layer was insufficient to cause a significant reduction of the forces in subsequent tests. Further experiments are needed to explore this hypothesis.

Thus, a decrease in insect adhesion on the *N. alata* wax coverage might not be solely explained by roughness exposed to the insect pads, as has been suggested by Scholz et al.[17]. It is possibly caused primarily by the breaking off of wax crystals from the upper wax layer that acts as a separation layer between the pad and the pitcher surface.

Methods

Preparation of test surfaces. The carnivorous plant species *Nepenthes alata* Blanco (Nepenthaceae), endemic to the Philippines, was used in our study[44]. Pitchers (Fig. 1A) were obtained from plants grown in the green house at the Botanical Garden of the Kiel University (Kiel, Germany). Fresh pitchers were harvested from four plants having the same genetic origin. The wax crystal structure in *N. alata*, which has been previously examined and documented extensively, has been shown to be very similar for every plant of this species studied so far[13,15,19,20]. This justifies the use of genetically similar plants in our study.

In order to minimize the effect of lunate cells, the lower part of the waxy zone located just above the transitional layer and bearing almost no lunate cells was used in all experiments. The untreated plant surface was used to investigate the upper wax layer (UL). To expose the lower wax layer (LL), the UL was mechanically removed by treating the waxy zone with a two-component polyvinylsiloxane (Coltène Whaledent Dentalvertriebs GmbH., Konstanz, Germany). Fluid polyvinylsiloxane was applied to the pitcher surface and then peeled off after 5 min of polymerization.

As reference surfaces, two epoxy resin[45] samples, smooth and micro-rough, were prepared. They were obtained from a smooth clean glass slide and micro-rough polishing paper with a defined asperity size of 3 μm (Serva Electrophoresis GmbH, Heidelberg, Germany) by applying a two-step molding method according to Gorb[46]. Data obtained on the smooth sample were used for further normalization of adhesion force values obtained on rough surfaces (see subsection *Adhesion tests* for details). Since the micro-rough epoxy resin sample exhibited roughness parameters similar to those of the intact wax coverage in *N. alata* (unpublished data), it was used as a solid micro-rough reference surface.

Characterisation of test surfaces and probes. *Microscopy.* The surface of plant and polymer samples as well as probes used in adhesion tests (see the subsection *Adhesion tests*) were examined before and after the tests in a scanning electron microscope (Hitachi S-4800, Hitachi High-Technologies Corporation, Tokyo, Japan). Pitcher surfaces and probes were investigated in a cryo-mode using Gatan ALTO 2500 cryo-preparation system (Gatan Inc., Abingdon, UK). A conventional SEM method was applied for examination of polymer replicas.

Small pieces of the plant material (0.5 cm × 0.5 cm) were cut out of the intact or treated waxy zone in *N. alata* pitchers (see *Preparation of test surfaces*) using a razor blade and then glued onto holders by means of polyvinyl alcohol Tissue-Tek

O.C.T.TM Compound (Sakura Finetek Europe B.V., Zoeterwoude, the Netherlands). In order to obtain fractures of the wax coverage, plant samples were placed vertically on specific holders and mechanically fixed. Afterwards, samples were frozen in liquid nitrogen and quickly transferred into a cryo-preparation chamber (133°K). For fractures, an integrated metal knife was applied. PDMS probes were attached to holders using conductive carbon double-sided adhesive tape and transferred, without previous treatment with liquid nitrogen, directly into the cryo-preparation chamber. All plant samples and polymer probes were sputter coated under frozen conditions with gold-palladium (1 : 9, 10 nm thick) and studied in SEM at 2 kV accelerating voltage. Small pieces of replicas were mounted on holders in the same way as the probes, sputter coated with gold–palladium (1 : 9, 10 nm thick) and examined in SEM at 7 kV accelerating voltage.

Roughness. The roughness of the test substrates was characterized by applying a white light interferometer (Zygo NewView 6000, Zygo Corporation, Middlefield, Connecticut, USA) at a 50× magnification (scanned area of 140 μm × 105 μm). R_a, r.m.s., and R_z were extracted from topographical height maps obtained. For this purpose, six measurements at different places on each surface were performed and the mean value and standard deviation were calculated for each roughness parameter.

Adhesion tests. Adhesion experiments were carried out with the micro-tribometer Basalt 01 (Tetra GmbH, Ilmenau, Germany) consisting of (1) a platform, (2) a metal spring with an attached probe and (3) a fiber-optic sensor (Fig. 6) (described in detail by Scherge and Gorb[47]). Tacky and deformable half-spherical indenters (probes) made out of PDMS according to Purtov et al.[31] were brought into contact at normal force ranging from 500 μN to 1000 μN with the test surface attached to the platform and then retracted at a constant speed of 37.6 ± 1 μm s^{-1}. The contact time of probes with surface, i.e. the time between the first contact and detachment, ranged from 4 s to 10 s. Using force - distance curves obtained, pull-off forces were measured (see Purtov et al.[31]). All experiments were carried out at room temperature (22–24°C) and a relative ambient humidity of 35–42%.

We carried out two types of experiments. First, three single measurements were performed with each probe on (1) the smooth replica, (2) the micro-rough replica and (3) one of the wax layer samples. The order of measurements was not randomized. Plant surfaces were prepared just before tests and immediately used for adhesion measurements. In total, 120 tests with 40 PDMS probes were carried out: respectively, 40 on the smooth and micro-rough replicas, 18 on the UL and 22 on the LL. We used normalized data for statistical comparison of the forces obtained on different test substrates. Using this approach, we avoided the influences of possible differences in tackiness of individual probes. In order to gain normalization, the force value of rough samples (micro-rough replica, UL and LL) was divided by that of the smooth reference surface measured with the same probe. In the case of the smooth reference, we normalized individual measurements on glass by the mean value of all forces measured on glass.

In order to test the effect of the contamination by wax crystals from the UL on adhesion forces, we carried out the second type of experiment. With the same probe, pull-off measurements were performed first on the smooth sample, then on the UL, and again on the smooth sample. We used 15 probes and carried out 45 tests in total. Force values were normalized to those obtained in the first test on the smooth sample.

Data obtained in the first type of experiment were statistically analyzed with Friedman repeated measures ANOVA on ranks. Multiple pairwise comparisons were performed using Wilcoxon signed rank test with Bonferroni correction. Force values measured in two tests on smooth sample in the second type of experiment were compared using paired t-test.

To prove the biological relevance of our experimental approach, we compared elastic properties of PDMS probes with material properties of insect adhesive pads and approximate pressure applied by probes to the plant surfaces with contact pressure of insects adhering to these surfaces. The elasticity modulus of the PDMS probes was calculated using the force - distance data obtained on smooth replica according to the 2-point method proposed by Ebenstein and Wahl[48], which is based on the Johnson-Kendall-Roberts theory[49]. In order to obtain the approximate pressure applied by the PDMS probe on the plant surfaces, we calculated the pressure (p) for a maximum and minimum load force according to Popov[50]:

$$p_{\min/\max} = \left(\frac{6F_{\min/\max}E^{*2}}{\pi^3 R^2}\right)^{1/3} \quad (1)$$

where F is the applied normal force (F_{min} = 0.5 mN and F_{max} = 1 mN), R is the radius of the polymer probe (1.5 mm) and E^* is the reduced E-modulus describing the elastic behavior of the contact system. The reduced E-modulus is related to Young's modulus (E_i) of solids as follows:

$$\frac{1}{E^*} = \frac{1-v_1^2}{E_1} + \frac{1-v_2^2}{E_2} \quad (2)$$

For the E-modulus of polymer probe (E_1), the value calculated as described above was used. For the plant surface, literature data on the digestive zone of the *N. alata* pitcher (E_2 = 637.19 kPa)[32] was entered into equation (2). For both the probe and plant surface, a Poisson ratio (v) of 0.5 was assumed[51,52].

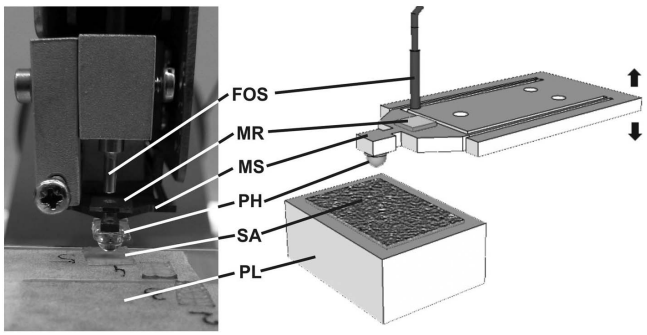

Figure 6 | Experimental set-up for adhesion tests. A test sample (SA) was mounted on a platform (PL). A soft indenter (PH), the sticky half-spherical probe made out of polydimethylsiloxane, was attached to a metal spring (MS). Driven by a motor, the sample and indenter were brought into contact and then retracted. Forces were detected using a fiber optic sensor (FOS) and a mirror (MR).

1. Juniper, B. E., Robins, R. J. & Joel, D. M. *The carnivorous plants* (Academic Press, London, 1989).
2. Beutel, R. G. & Gorb, S. N. Ultrastructure of attachment specializations of hexapods (Arthropoda): Evolutionary patterns inferred from a revised ordinal phylogeny. *J. Zool. Syst. Evol. Research* **39**, 177–207 (2001).
3. Gorb, S. *Attachment Devices of Insect Cuticle* (Kluwer Academic Publishers, Dordrecht, 2001).
4. Gorb, S. N. Smooth attachment devices in insects: Functional morphology and biomechanics. *Advan. Insect Physiol.* **34**, 81–115 (2007).
5. Adam, H. Prey spectra of Bornean *Nepenthes* species (Nepenthaceae) in relation to their habitat. *Pertanika J. Trop. Agric. Sci.* **20**, 121–134 (1997).
6. Moran, J. A. Pitcher dimorphism, prey composition and the mechanisms of prey attraction in the pitcher plant *Nepenthes rafflesiana* in Borneo. *J. Ecol.* **84**, 515–525 (1996).
7. Moran, J. A., Booth, W. E. & Charles, J. K. Aspects of pitcher morphology and spectral characteristics of six Bornean *Nepenthes* pitcher plant species: Implications for prey capture. *Ann. Bot.* **83**, 521–528 (1999).
8. Owen, T. P. & Lennon, K. A. Structure and development of the pitchers from the carnivorous plant *Nepenthes alata* (Nepenthaceae). *Am. J. Bot.* **86**, 1382–1390 (1999).
9. Gaume, L., Gorb, S. & Rowe, N. Function of epidermal surfaces in the trapping efficiency of *Nepenthes alata* pitchers. *New Phytol.* **156**, 479–489 (2002).
10. Moran, J. A. & Clarke, C. M. The carnivorous syndrome in *Nepenthes* pitcher plants: Current state of knowledge and potential future directions. *Plant Signal. Behav.* **5**, 644–648 (2010).
11. Juniper, B. E. & Burras, J. K. How pitcher plant trap insects. *New Sci.* **269**, 75–77 (1962).
12. Riedel, M., Eichner, A. & Jetter, R. Slippery surfaces of carnivorous plants: composition of epicuticular wax crystals in *Nepenthes alata* Blanco pitchers. *Planta* **218**, 87–97 (2003).
13. Gorb, E. *et al.* Composite structure of the crystalline epicuticular wax layer of the slippery zone in the pitchers of the carnivorous plant *Nepenthes alata* and its effect on insect attachement. *J. Exp. Biol.* **208**, 4651–4662 (2005).
14. Riedel, M., Eichner, A., Meimberg, H. & Jetter, R. Chemical composition of epicuticular wax crystals on the slippery zone in pitchers of five *Nepenthes* species and hybrids. *Planta* **225**, 1517–1534 (2007).
15. Gorb, E. & Gorb, S. [Functional surfaces in the pitcher of the carnivorous plant *Nepenthes alata*: a cryo-SEM approach] *Functional Surfaces in Biology: Adhesion Related Effects* [Gorb, S. N.(ed.)] [205–238] (Springer, Dordrecht, 2009).
16. Poppinga, S., Koch, K., Bohn, H. F. & Barthlott, W. Comparative and functional morphology of hierarchically structured anti-adhesive surfaces in carnivorous plants and kettle trap flowers. *Funct. Plant Biol.* **37**, 952–961 (2010).
17. Scholz, I. *et al.* Slippery surfaces of pitcher plants: *Nepenthes* wax crystals minimize insect attachment via microscopic surface roughness. *J. Exp. Biol.* **213**, 1115–1125 (2010).
18. Wang, L. & Zhou, Q. Numerical characterization of surface structures of slippery zone in *Nepenthes alata* pitchers and its mechanism of reducing locust's attachment. *Adv. Nat. Sci.* **3**, 152–160 (2010).
19. Gorb, E. V. & Gorb, S. N. The effect of surface anisotropy in the slippery zone of *Nepenthes alata* pitchers on beetle attachment. *Beilstein J. Nanotechnol.* **2**, 302–310 (2011).
20. Benz, M. J., Gorb, E. V. & Gorb, S. N. Diversity of the slippery zone microstructure in pitchers of nine carnivorous *Nepenthes* taxa. *Arthropod-Plant Interact.* **6**, 147–158 (2012).
21. Bonn, H. F. & Federle, W. Insect aquaplaning: *Nepenthes* pitcher plants capture prey with the peristome, a fully wettable water-lubricated anisotropic surface. *Proc. Natl. Acad. Sci. USA* **101**, 14138–14143 (2004).

22. Bauer, U., Bohn, H. F. & Federle, W. Harmless nectar source or deadly trap: *Nepenthes* pitchers are activated by rain, condensation and nectar. *Proc. R. Soc. B* **275**, 259–265 (2008).
23. Gaume, L. & Forterre, Y. A viscoelastic deadly fluid in carnivorous pitcher plants. *PLoS ONE* **11**, e1185 (2007).
24. DiGiusto, B., Grosbois, V., Fargeas, E., Marshall, D. J. & Gaume, L. Contribution of pitcher fragrance and fluid viscosity to high prey diversity in a *Nepenthes* carnivorous plant from Borneo. *J. Biosci.* **33**, 121–136 (2008).
25. Bonhomme, V., Pelloux-Prayer, H., Jousselin, E., Forterre, Y., Labat, J.-J. & Gaume L. 2011 - Slippery or sticky? Functional diversity in the trapping strategy of *Nepenthes* carnivorous plants. *New Phytol.* **191**, 545–554 (2011).
26. Bauer, U., Clemente, C. J., Renner, T. & Federle, W. (2012). Form follows function: morphological diversification and alternative trapping strategies in carnivorous *Nepenthes* pitcher plants. *J. Evolution. Biol.* **25**, 90–102 (2012).
27. Gorb, E. V., Baum, M. J. & Gorb, S. N. Development and regeneration ability of the wax coverage in *Nepenthes alata* pitchers: a cryo-SEM approach. *Sci. Rep.* **3**, 3078 (2013).
28. Gaume, L. *et al.* How do plant waxes cause flies to slide? Experimental tests of wax-based trapping mechanisms in three pitfall carnivorous plants. *Athropod Struct. Dev.* **33**, 103–111 (2004).
29. Gorb, E. V. & Gorb, S. N. Attachment ability of the beetle *Chrysolina fastuosa* on various plant surfaces. *Entomol. Exp. Appl.* **105**, 13–28 (2002).
30. Martin, J. T. & Juniper, B. E. *The Cuticles of Plants* (Edward Arnold, London, 1970).
31. Purtov, J., Gorb, E. V., Steinhart, M. & Gorb, S. N. Measuring of hardly measurable: adhesion properties of anti-adhesive surfaces. *Appl. Phys. A* **111**, 183–189 (2013).
32. Gorb, E. *et al.* Structure and properties of the glandular surface in the digestive zone of the pitcher in the carnivorous plant *Nepenthes ventrata* and its role in insect trapping and retention. *J. Exp. Biol.* **207**, 2947–2963 (2004).
33. Gorb, E. & Gorb, S. Effects of surface topography and chemistry of *Rumex obtusifolius* leaves on the attachment of the beetle *Gastrophysa viridula*. *Entomol. Exp. Appl.* **130**, 222–228 (2009).
34. Gorb, S., Jiao, Y. & Scherge, M. (2000) Ultrastructural architecture and mechanical properties of attachment pads in *Tettigonia viridissima* (Orthoptera, Tettigoniidae). *J. Comp. Physiol. A* **186**, 821–831 (2000).
35. Scholz, I., Baumgartner, W. & Federle, W. Micromechanics of smooth adhesive organs in stick insects: pads are mechanically anisotropic and softer towards the adhesive surface. *J. Comp. Physiol. A* **194**, 373–384 (2008).
36. Persson, B. N. J. On the theory of rubber. *Surf. Sci.* **401**, 445–454 (1998).
37. Fuller, K. N. G. & Tabor, D. The effect of surface roughness on the adhesion of elastic solids. *Proc. R. Soc. Lond. A* **345**, 327–342 (1975).
38. Briggs, G. A. D. & Briscoe, B. J. The effect of surface topography on the adhesion of elastic solids. *J. Phys. D: Appl. Phys.* **10**, 2453–2466 (1977).
39. Peressadko, A., Hosoda, N. & Persson, B. N. J. Influence of surface roughness on adhesion between elastic bodies. *Phys. Rev. Lett.* **95**, 124301 (2005).
40. Peisker, H., Michels, J. & Gorb, S. N. Beetles in rubber boots - evidence for a material gradient in the adhesive tarsal setae. *Nat. Commun.* **4**, 1661 (2013).
41. Borodich, F. M., Gorb, E. V. & Gorb, S. N. Fracture behaviour of plant epicuticular wax crystals and its role in preventing insect attachment: A theoretical approach. *Appl. Phys. A* **100**, 63–71 (2010).
42. Homola, A. M., Israelachvili, J. N., Gee, M. L. & McGuiggan, P. M. Measurements of and relation between the adhesion and friction of two surfaces separated by molecularly thin liquid films. *J. Tribol.* **111**, 675–682 (1989).
43. Persson, B. N. J. & Tosatti, E. The effect of surface roughness on the adhesion of elastic solids. *J. Chem. Phys.* **115**, 5597–5610 (2001).
44. McPherson, S. *Pitchers Plants of the World* (Redfern Natural History Productions, Poole, 2009).
45. Spurr, A. R. A low-viscosity epoxy resin embedding medium for electron microscopy. *J. Ultrastruct. Res.* **26**, 31–43 (1969).
46. Gorb, S. N. Visualisation of native surfaces by two-step molding. *Microsc. Today* **15**, 44–46 (2007).
47. Scherge, M. & Gorb, S. N. *Biological Micro- and Nanotribology* (Springer, Berlin, 2000).
48. Ebenstein, D. M. & Wahl, K. J. A comparison of JKR-based methods to analyze quasi-static and dynamic indentation force curves. *J. Colloid Interface Sci.* **298**, 652–662 (2006).
49. Johnson, K. L., Kendall, K. & Roberts, A. D. Surface energy and the contact of elastic solids. *Proc. R. Soc. Lond. A* **324**, 301–313 (1971).
50. Popov, V. L. Contact Mechanics and Friction: Physical Principles and Applications (Springer, Heidelberg, 2010).
51. Fung, Y. C. Biomechanics Mechanical Properties of Living Tissues (Springer, New York, 1993).
52. Mark, J. E. *Polymer Data Handbook* (Oxford University Press, New York, 1999).

Acknowledgments

We are very grateful to Nadine Jacky (Kiel University, Kiel, Germany) for her help with performing the second type of adhesion tests. Many thanks to Dr. Alexander Kovalev and Lars Heepe (both Kiel University, Kiel, Germany) for providing the calculation program for E-modulus and formulae for evaluation of the pressure applied by insects to the plant surface, respectively. The plant material was provided by the staff of the Botanical Garden at the Kiel University. Vicky Kastner (Tübingen, Germany) helped with linguistic corrections of the manuscript. This study was partly supported by the SPP 1420 priority program of the German Science Foundation (DFG) 'Biomimetic Materials Research: Functionality by Hierarchical Structuring of Materials' [GO 995/9-2 to SG].

Author contributions

The authors contributed equally to designing of experiments. J.P. performed SEM and roughness examinations, measured pull-off forces in the first type of adhesion test and analyzed the data obtained. E.V.G. completed measurements and analyses. E.V.G. and J.P. wrote the manuscript. S.N.G. contributed to interpretation of the findings and provided corrections of the manuscript.

Additional information

Competing financial interests: The authors declare no competing financial interests.

How to cite this article: Gorb, E.V., Purtov, J. & Gorb, S.N. Adhesion force measurements on the two wax layers of the waxy zone in *Nepenthes alata* pitchers. *Sci. Rep.* **4**, 5154; DOI:10.1038/srep05154 (2014).